Tran-SET

Transportation Consortium of South-Central States

Solving Emerging Transportation Resiliency, Sustainability, and Economic Challenges through the Use of Innovative Materials and Construction Methods: From Research to Implementation

Development of Novel Ultra-High Performance Engineered Cementitious Composites (UHP-ECC) for Durable and Resilient Transportation Infrastructure

Project No. 20CLSU08

Lead University: Louisiana State University

Final Report

September 2021

Disclaimer

The contents of this report reflect the views of the authors, who are responsible for the facts and the accuracy of the information presented herein. This document is disseminated in the interest of information exchange. The report is funded, partially or entirely, by a grant from the U.S. Department of Transportation's University Transportation Centers Program. However, the U.S. Government assumes no liability for the contents or use thereof.

Acknowledgements

The authors would like to acknowledge the financial support for this study by the Transportation Consortium of South-Central States (Tran-SET) and the Louisiana Transportation Research Center (LTRC).

TECHNICAL DOCUMENTATION PAGE

1. Project No.	**2. Government Accession No.**	**3. Recipient's Catalog No.**
20CLSU08		
4. Title and Subtitle		**5. Report Date** Sep. 2021
Development of Novel Ultra-High Performance Engineered Cementitious Composites (UHP-ECC) for Durable and Resilient Transportation Infrastructure		**6. Performing Organization Code**
7. Author(s) PI: Gabriel A. Arce https://orcid.org/0000-0002-3610-8238 Co-PI: Marwa M. Hassan https://orcid.org/0000-0001-8087-8232 GRA: Daniel Game		**8. Performing Organization Report No.**
9. Performing Organization Name and Address Transportation Consortium of South-Central States (Tran-SET)		**10. Work Unit No. (TRAIS)**
University Transportation Center for Region 6 3319 Patrick F. Taylor Hall, Louisiana State University, Baton Rouge, LA 70803		**11. Contract or Grant No.** 69A3551747106
12. Sponsoring Agency Name and Address United States of America Department of Transportation		**13. Type of Report and Period Covered** Final Research Report Aug. 2020 – Sep. 2021
Research and Innovative Technology Administration		**14. Sponsoring Agency Code**

15. Supplementary Notes

Report uploaded and accessible at Tran-SET's website (http://transet.lsu.edu/).

16. Abstract

The objective of this study was to develop novel UHP-ECC materials utilizing readily available ingredients in Region 6 for the construction and repair of transportation infrastructure. Phase one of this study focused on the development of ultra-high strength cementitious matrices by evaluating the effects of ingredient selection and mixture proportioning on the materials' compressive strength. Variables evaluated included the mass ratios of silica fume to fly ash (SF/FA), supplementary cementitious materials to cement (SCMs/C), and ordinary sand to microsilica sand (OS/MS). Phase two of the study focused on the development of UHP-ECC materials. To this end, based on the knowledge gained from phase one, two ultra-high strength cementitious matrices (one with and one without SF) were formulated and their fracture properties were evaluated through fracture toughness test. Furthermore, fiber-bridging properties of ultra-high-molecular-weight (UHMW) polyethylene (PE) fiber in the developed cementitious matrices were evaluated through single crack tensile test (SCTT). Four different composites were produced by reinforcing the selected cementitious matrices with 1.5 and 2 vol.% UHMW PE fiber. Fresh and hardened properties of the developed composites were assessed by means of flowability test, compressive strength test, uniaxial tensile test, and flexural performance test. Results from phase one showed that SF/FA had the most relevant effect on compressive strength, followed by SCMs/C, and OS/MS. Furthermore, increments in SF/FA produced improvements in strength, whereas increments in SCMs/C and OS/MS reduced strength. Experimental results from phase two indicated that the use of SF and the increase in fiber content generally had a negative effect on the fresh and hardened properties of the composites. These observations were credited to a worsening fiber distribution when using silica fume and/or increasing fiber content. Three UHP-ECC materials utilizing readily available ingredients were successfully developed (i.e., mixtures FA_{25}-$f_{1.5}$, FA_{25}-f_2, and $FA_{20}SF_5$-f_2). These materials simultaneously exhibited ultra-high compressive strength (>120 MPa) and ECC-like ductility (tensile strain capacity >2%). The average crack width for all mixtures ranged between 61-131 µm. Mixture FA_{25}-$f_{1.5}$, which displayed the best mechanical properties, exhibited a compressive strength of 133.1 MPa, flexural strength of 21.4 MPa, tensile strength of 10.3 MPa, tensile strain capacity of 4.3%, and an average crack width of 115.3 µm. Importantly, this mixture did not incorporate silica fume or microsilica sand and used low fiber content (i.e., 1.5 vol.%).

17. Key Words	**18. Distribution Statement**
Concrete, fibers, UHPC, ECC, UHP-ECC, pseudo strain hardening, transportation infrastructure	No restrictions. This document is available through the National Technical Information Service, Springfield, VA 22161.

19. Security Classif. (of this report)	**20. Security Classif. (of this page)**	**21. No. of Pages**	**22. Price**
Unclassified	Unclassified	33	

Form DOT F 1700.7 (8-72) **Reproduction of completed page authorized.**

SI* (MODERN METRIC) CONVERSION FACTORS

APPROXIMATE CONVERSIONS TO SI UNITS

Symbol	When You Know	Multiply By	To Find	Symbol
		LENGTH		
in	inches	25.4	millimeters	mm
ft	feet	0.305	meters	m
yd	yards	0.914	meters	m
mi	miles	1.61	kilometers	km
		AREA		
in^2	square inches	645.2	square millimeters	mm^2
ft^2	square feet	0.093	square meters	m^2
yd^2	square yard	0.836	square meters	m^2
ac	acres	0.405	hectares	ha
mi^2	square miles	2.59	square kilometers	km^2
		VOLUME		
fl oz	fluid ounces	29.57	milliliters	mL
gal	gallons	3.785	liters	L
ft^3	cubic feet	0.028	cubic meters	m^3
yd^3	cubic yards	0.765	cubic meters	m^3
		NOTE: volumes greater than 1000 L shall be shown in m^3		
		MASS		
oz	ounces	28.35	grams	g
lb	pounds	0.454	kilograms	kg
T	short tons (2000 lb)	0.907	megagrams (or "metric ton")	Mg (or "t")
		TEMPERATURE (exact degrees)		
^oF	Fahrenheit	5 (F-32)/9 or (F-32)/1.8	Celsius	^oC
		ILLUMINATION		
fc	foot-candles	10.76	lux	lx
fl	foot-Lamberts	3.426	candela/m^2	cd/m^2
		FORCE and PRESSURE or STRESS		
lbf	poundforce	4.45	newtons	N
lbf/in^2	poundforce per square inch	6.89	kilopascals	kPa

APPROXIMATE CONVERSIONS FROM SI UNITS

Symbol	When You Know	Multiply By	To Find	Symbol
		LENGTH		
mm	millimeters	0.039	inches	in
m	meters	3.28	feet	ft
m	meters	1.09	yards	yd
km	kilometers	0.621	miles	mi
		AREA		
mm^2	square millimeters	0.0016	square inches	in^2
m^2	square meters	10.764	square feet	ft^2
m^2	square meters	1.195	square yards	yd^2
ha	hectares	2.47	acres	ac
km^2	square kilometers	0.386	square miles	mi^2
		VOLUME		
mL	milliliters	0.034	fluid ounces	fl oz
L	liters	0.264	gallons	gal
m^3	cubic meters	35.314	cubic feet	ft^3
m^3	cubic meters	1.307	cubic yards	yd^3
		MASS		
g	grams	0.035	ounces	oz
kg	kilograms	2.202	pounds	lb
Mg (or "t")	megagrams (or "metric ton")	1.103	short tons (2000 lb)	T
		TEMPERATURE (exact degrees)		
^oC	Celsius	1.8C+32	Fahrenheit	^oF
		ILLUMINATION		
lx	lux	0.0929	foot-candles	fc
cd/m^2	candela/m^2	0.2919	foot-Lamberts	fl
		FORCE and PRESSURE or STRESS		
N	newtons	0.225	poundforce	lbf
kPa	kilopascals	0.145	poundforce per square inch	lbf/in^2

TABLE OF CONTENTS

LIST OF FIGURES

LIST OF TABLES

ACRONYMS, ABBREVIATIONS, AND SYMBOLS

ANOVA	Analysis of Variance
ASTM	American Society for Testing and Materials
C3DP	Construction 3D Printing
ECC	Engineered Cementitious Composites
FA	Fly Ash
HPFRCC	High-Performance Fiber-Reinforced Cementitious Composites
HRWR	High Range Water Reducer
ITZ	Interfacial Transition Zone
LSU	Louisiana State University
MS	Microsilica Sand
OPC	Ordinary Portland cement
OS	Ordinary Sand
PSH	Pseudo Strain Hardening
SCM	Supplementary Cementitious Material
SF	Silica Fume
UHPC	Ultra-High-Performance Concrete
UHP-ECC	Ultra-High-Performance Engineered Cementitious Composites
XRD	X-ray Diffraction
XRF	X-ray Fluorescence

EXCECUTIVE SUMMARY

Ultra-High Performance Engineered Cementitious Composites (UHP-ECCs) are novel concrete materials simultaneously exhibiting exceptional mechanical strength and ductility. The design of these cementitious composites are grounded on the fracture mechanics and micromechanics design concepts of ECC and the dense particle packing design concepts of Ultra-High Performance Concrete (UHPC). While UHP-ECCs are promising for civil infrastructure, their formulation often includes microsilica sand (which is expensive and not readily available), expensive SCMs such as silica fume, and relatively high contents of fiber (i.e., 2 vol.%), which limit their cost-effectiveness and practicality. As a response, the aim of this study was to develop novel UHP-ECC materials utilizing ingredients that are readily available in Region 6 for the construction and repair of transportation infrastructure. To this end, the study was conducted in two phases. First the effect of ingredient selection and mixture proportioning on the cementitious-matrices' strength was thoroughly investigated. The variables studied were the mass ratios of supplementary cementitious materials to cement (SCMs/C), silica fume to fly ash (SF/FA), and ordinary sand to microsilica sand (OS/MS). A total of 36 cementitious matrices with 3 specimens each (i.e., 108 specimens) were prepared and evaluated in compression according to ASTM C109. Next, the second phase of the study focused on the development of UHP-ECCs and used the knowledge gathered in the first phase of the study to design cementitious matrices with appropriate strength for the application. In the development of UHP-ECCs, the effect of silica fume and fiber content was assessed on the fresh and hardened properties the materials. Tests conducted on the composites included the flow table test (ASTM C1437), compressive strength test (ASTM C109), uniaxial tensile test (according to JSCE recommendations), and flexural performance test (ASTM C1609). In addition, matrix fracture properties and composite fiber-bridging properties were evaluated by means of notched-beam fracture toughness tests (according to the effective crack model, i.e., ECM) and single-crack tensile tests (SCTT), respectively.

Experimental results from the first phase of the study indicated that the SF/FA ratio had the most important effect on the cementitious-matrices' compressive strength, followed by the ratio of SCMs/C, and lastly the ratio of OS/MS, which had a very small effect on strength. Moreover, increments in the SF/FA ratio produced strength improvements, whereas increments in the ratios of SCMs/C and OS/MS produced strength decrements. A compressive strength prediction model utilizing as input the ratios of SCMs/C, SF/FA, and OS/MS was created using multiple linear regression. In turn, the compressive strength prediction model was used as a guidance for the production of UHP-ECC cementitious matrices.

In terms of fresh properties, results from phase two of the study revealed that the use of SF and augmenting fiber content from 1.5 to 2 vol.% resulted in decrements in the workability of the fresh mixtures. In the case of mixtures implementing 2% fiber content, some fiber clumps were detected by visual inspection and touch of the fresh mixture. This was particularly the case for mixtures implementing SF. In terms of hardened properties, the incorporation of SF tended to decrease the compressive strength of the composites, whereas the increase in fiber content did not produce any obvious tendency in strength. Notwithstanding, differences in strength observed were not statistically significant. Importantly, the compressive strength of the composites developed ranged from 115.8 to 133.1 MPa with three out of the four different mixtures assessed presenting strengths greater than 120 MPa. All the composites evaluated exhibited ECC-like ductility (i.e., >2% tensile strain capacity), which was consistent with the PSH strength and PSH energy indexes obtained

from matrix fracture properties (i.e., J_{tip} and σ_{cr}) and composite fiber-bridging properties (i.e., σ_0 and J'_b) obtained experimentally for each mixture. Surprisingly, the use of SF and the increase in fiber content generally produced adverse effects in the tensile strength and strain capacity of the materials (differences not statistically significant for strain capacity), which contradicted expected composite response from σ_0 and PSH indexes obtained. These observations were credited to a worsening fiber distribution as silica fume was incorporated and/or fiber content was increased, which deteriorated the tensile performance of the composites. The average crack width of the materials ranged between 61-131 μm, while the average number of cracks ranged between 18.2-31.0. Mixtures that did not contain SF resulted in a fewer number of cracks, which agreed with the attained tensile strain capacity. Flexural performance of the materials produced similar tendencies as those observed for the tensile performance, however no statistically significant differences in flexural strength and deflection capacity were encountered between mixtures. All the composites exhibited a deflection hardening behavior with the flexural strength ranging from 20.9 to 24.4 MPa.

From the results obtained in this study, three UHP-ECC materials utilizing readily available ingredients were successfully developed (i.e., mixtures FA_{25}-$f_{1.5}$, FA_{25}-f_2, and $FA_{20}SF_5$-f_2). These materials simultaneously exhibited ultra-high compressive strength (>120 MPa) and high tensile ductility (tensile strain capacity >2%). It is important to indicate that composite FA_{25}-$f_{1.5}$, which generally presented the best mechanical properties, exhibited a compressive strength of 133.1 MPa (i.e., ~4.5 times that of concrete), flexural strength of 21.4 MPa (~4 times that of concrete), tensile strength of 10.3 MPa (~3 times that of concrete), and tensile strain capacity of 4.3% (~430 times that of concrete). Importantly, mixture FA_{25}-$f_{1.5}$ does not require the use of silica fume or microsilica sand and utilizes low fiber content (i.e., 1.5 vol.%). In turn, this makes this UHP-ECC more practical and cost-effective than previous versions of the material.

1. INTRODUCTION

Ultra-high-performance concrete (UHPC) is a concrete material with high strength (i.e., a minimum specified compressive strength of 120 MPa) and excellent durability *(1, 2)*. To produce high strength, UHPC materials are prepared utilizing high cement content (i.e., over 800 kg/m^3), low water/binder ratio (i.e., lower than 0.2), and a high particle packing density design approach *(2, 3)*. UHPCs usually include short randomly distributed discrete fibers (typically steel fibers at 2 to 6% vol.) *(4)*. In turn, this provides UHPCs with enhanced tensile properties and can allow for moderate strain-hardening capabilities when using high fiber content; yet, the ductility of these composites remains limited (usually about 0.6% strain capacity in tension) and crack width relatively large (i.e., over 100 µm)*(5)*.

Figure 1. Ductile behavior of ECC material developed at LSU *(6)*

Engineered Cementitious Composites (ECCs) also known as bendable concrete (Figure 1), are a novel class of high-performance fiber-reinforced cementitious composites (HPFRCC) that are designed based on micromechanics and fracture mechanics principles to display a highly pseudo ductile response at small fiber contents of 1 to 2 vol.% *(7)*. This make ECCs practical to be implemented in the field using existing equipment and techniques as well as significantly more cost-effective than early versions of HPFRCC. ECCs ductility occurs through a process of multiple steady-state micro-cracks formation referred to as pseudo strain hardening (PSH). In contrast to the limited deformation capacity of typical HPFRCC (i.e., often below 1% strain capacity in tension), ECCs exhibit a tensile strain capacity ranging from 1 to 8% (i.e., 100 to 800 times that of concrete). Nonetheless, typical ECCs exhibit a tensile strain capacity of 2 to 5%*(8)*. Due to its superior mechanical properties (i.e., high tensile ductility and tight crack width), ECCs perform well against relevant deterioration mechanisms in concrete structures (i.e., alkali-silica reaction, sulfate attack, freeze-thaw, corrosion) *(7, 9)*. Importantly, autogenous healing mechanisms of cementitious materials are effective at healing microcracks in ECCs, thus further supporting ECCs' excellent durability characteristics *(10)*.

For the design of structures, both strength and ductility of structural materials are of utmost importance to ensure safety and reliability of structures, particularly at extreme conditions. As such, endowing concrete with high strength and ductility capabilities could potentially allow for the design of civil infrastructure with concrete as the solo structural material. Recently, Ultra-High-Performance ECC (UHP-ECC) materials have been proposed to overcome the limited ductility of UHPC and produce cementitious composites with remarkable mechanical properties *(3, 11, 12)*. The design of this emerging class of concrete materials are based on the combination of the micromechanics and fracture mechanics design concepts of ECC and the high particle packing density matrix design approach of UHPC. Through the combination of these, high strength and high ductility can be simultaneously achieved. For instance, in a recent study by Yu et al. *(3)*, an UHPC-ECC composite was developed with a compressive strength of 121.5 MPa and a tensile strain capacity of more than 8% (i.e., comparable to that of some metals) as shown in Table 1. Consequently, this opens the possibility of designing and constructing infrastructure with UHP-ECC as the solo structural material. Furthermore, UHP-ECC materials are excellent candidates to be implemented in additive manufacturing, allowing for 3-D printing of robust infrastructure.

Table 1. Properties of concrete materials

Properties	**Regular Concrete**	**UHPC-FRC *(5, 13–17)***	**UHP-ECC *(3)***
Compressive Strength (MPa)	30	150-230	121.5
Tensile Strength (MPa)	3.2	9-19.6	17.4
Tensile Strain Capacity (%)	0.01	0.24-0.64	8.2
Crack width (μm)	N/A	>100	<100

2. OBJECTIVES

The objective of this study was to develop novel UHP-ECC materials utilizing ingredients that are readily available in Region 6. The development of such materials will provide the region with state-of-the-art cementitious composites that will be available for the construction and repair of transportation infrastructure as well as for future research such as the implementation of these materials in construction 3D printing (C3DP).

3. LITERATURE REVIEW

3.1. Design Principles of UHPC

The main principles driving the design of UHPC are the reduction in porosity, dense particle packing, microstructure enhancement, improved toughness, and homogeneity enhancement *(18)*.

3.1.1. Reduction in Porosity

The porosity and compressive strength of concrete have a direct relationship, i.e., the lower the porosity, the higher the strength. In addition, a decrease in porosity improves the durability of concrete as it provides high resistance against penetration of deleterious substances into the material. Apart from the total porosity of concrete, the pore size distribution, shape and position of the pores also play a role in the mechanical strength of concrete *(18)*. In UHPC, the reduction in pore size and its improved distribution can be achieved through the incorporation of very fine reactive mineral admixture, use of superplasticizer, lower water to cement ratio (w/c) and close packing of raw materials *(18, 19)*. Some of these factors are discussed in the following subsections.

3.1.2. Packing of Raw Materials

The main design principle of UHPC is to achieve a densely compacted cementitious matrix that yields high mechanical strength and adequate workability. Different particle packing models have been used by various researchers for the design of UHPC. For instance, some researchers used Andreasen and Andersen's model for the optimization of matrix composition *(20, 21)*. Similarly, an optimization algorithm based on the Least Squares Model has been used to proportion the raw materials in the mixture *(18)*. The Packing density model, Compressive Packing Model, Aim and Goff's model, and D-optimal design are other models that have been used in previous studies *(22–25)*

3.1.3. Reduction in w/c Ratio

Lowering w/c ratio will decrease the porosity in hydrated cement paste, and will subsequently increase the compressive strength of hardened concrete *(26)*. In UHPC, the range of w/c ratio is 0.14-0.20, which is significantly lower than the w/c ratio of normal cementitious composites, i.e., 0.4-0.5 *(18)*. Since w/c is reduced in UHPC, superplasticizers are used in the mix to achieve adequate workability for material processing. Hence, the selection of superplasticizer is one of the critical steps in the production of UHPC.

3.1.4. Improved Toughness

In contrast to conventional concrete, UHPC generally implement steel fibers which produces an improved toughness (i.e., the energy absorption capacity of the material and its ability to resist fracture) *(27)*. Incorporation of fibers in UHPC not only prevents and controls the initiation of cracks but also resists the propagation of cracks. This is achieved through the fiber bridging capacity of fibers which transfer the load through the interface between the matrix and fibers *(28)*. From previous studies, it has been observed that the steel fibers dramatically improve the toughness of UHPC *(18, 29, 30)*.

3.1.5. Microstructure Enhancement

UHPC exhibits enhanced mechanical properties due to its uniform and very dense microstructure *(18)*. Improvement in UHPC microstructure is achieved due to the close packing density, incorporation of pozzolanic materials, lower w/c ratio, and fewer voids in the interfacial transition zone (ITZ) *(18, 31)*. The microstructure of UHPC, consists mainly of hydration products (mainly calcium silicate hydrate, i.e., C-S-H), un-hydrated cement, and minimal pores *(31)*. These pores range from 2-3 nm with a total porosity of about 2.23% *(18)*. However, when cured at higher temperatures, i.e., 150-200°C, the pore space in UHPC becomes negligible. This is due to the accelerated pozzolanic reaction between calcium hydroxide (CH) and pozzolanic materials, which fills the voids by the formation C-S-H gel *(31, 32)*. Furthermore, an X-ray diffraction (XRD) analysis conducted in a study by Wang et al. showed that the hydrated cement paste has no ettringite and minimal CH *(31)*. The ITZ is the weak zone in conventional concrete where most of the failure occurs due to its high porosity and high CH content. However, in UHPC, the ITZ is as dense as the matrix due to the low w/c ratio and high C-S-H content. It is also important to note that the density of the C-S-H gel in UHPC is higher than in conventional concrete *(18)*. This improved and dense microstructure is an important factor in the performance of UHPC.

3.1.6. Improvement in Homogeneity

In UHPC the utilization of very fine quartz sand instead of conventional aggregates decreases the formation of microcracks and results in the ITZ being as dense as the matrix *(33)*. Furthermore, the incorporation of fine sand decreases both the defects and inhomogeneity in UHPC. This, in turn, reduces the failure of concrete along the ITZ and enhances the durability due to the absence of microcracks in the ITZ *(18)*. Therefore, the homogenous microstructure is a vital parameter for the performance of UHPC.

3.2. Design Principles of ECC

The design and optimization of ECC materials are based on micromechanics and fracture mechanics concepts. The implementation of these concepts allow for the design of composites exhibiting PSH behavior at relatively low fiber contents *(34)*. There are two fundamental criteria that must be satisfied for the PSH behavior of ECC to occur, the strength criterion and the energy criterion *(35)*. These criteria will be discussed in the subsections below.

3.2.1. Strength Criterion

The strength criterion guarantees that there is appropriate fiber-bridging capacity when cracks initiate from any defect site in the composite. To this end, the matrix first-cracking strength (σ_{cr}) should not exceed the fiber-bridging capacity (σ_0) on any possible crack plane as illustrated by Equation 1 *(36)*:

$$\sigma_0 \geq \sigma_{cr} \tag{1}$$

where,

σ_0= Fiber-bridging capacity;

σ_{cr}= Matrix cracking strength.

If this condition is not satisfied, fibers will rupture and/or pull out of the matrix upon the initiation of a crack leading to failure of the composite.

3.2.2. *Energy Criterion*

The energy criterion guarantees the occurrence of steady-state flat-crack propagation *(37)*. The energy criterion essentially requires energy equilibrium in the system which allows the propagation of cracks at constant tensile stress (σ_{ss}) while maintaining a uniform opening of cracks (δ_{ss}) with the exception of the small zone in the wake of the crack tip *(38)*. The energy criterion is satisfied when the complementary energy of the fiber-bridging relation (J_b') is higher than the crack tip matrix toughness (J_{tip}). Figure 2a illustrates J_{tip} and J'_b in a fiber-bridging relation curve. The energy criteria was first recognized by Marshall and Cox through J-integral analysis and is presented in the following equation *(8, 35, 39)*:

$$J'_b = \sigma_0\delta_0 - \int_0^{\delta_0} \sigma(\delta)\, d\delta \ \geq \ J_{tip} \tag{2}$$

where,

J'_b = Complementary energy of the fiber-bridging relation;

J_{tip}= Crack-tip matrix toughness;

δ_0= Crack opening corresponding to σ_0;

$\sigma(\delta)$= Fiber-bridging relationship.

The strength and energy criteria are generally presented in the form of PSH indexes (i.e., σ_0/σ_{cs} and J_b'/J_{tip} ratios). If either the PSH strength or PSH energy index is lower than one, the composites will exhibit a single crack softening response rather than a strain-hardening multiple crack behavior (see Figure 2b). It is imperative to understand that Equation 1 and Equation 2 consider an homogeneous material; hence, in fact the necessity for PSH indexes larger than one is necessary for robust PSH performance *(8, 40)*. Kanda and Li *(41)* suggested PSH strength index and PSH energy index of 1.3 and 2.7, respectively, to ensure saturated PSH behavior of the composites. Saturated PSH behavior refers to the ultimate multiple cracking concentration which can occur in the composite before crack spacing is too small for further formation of cracks (because of inadequate stress transfer from fibers at a crack plane) *(42)*.

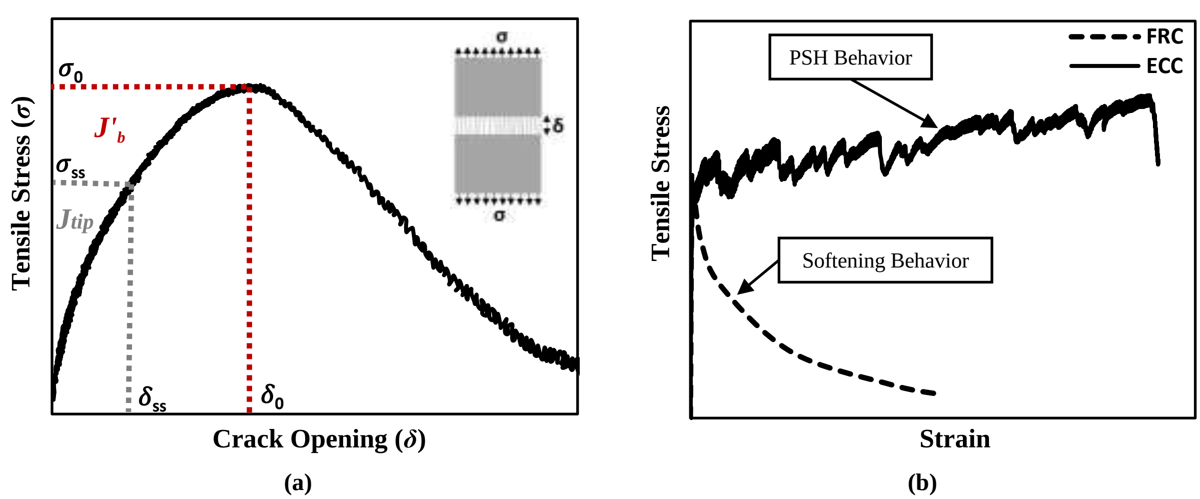

Figure 2. (a) Fiber bridging relation (σ-δ curve), and (b) stress vs. strain behavior of ECC and FRC in tension (adapted from)

3.3. UHP-ECC

An emerging concrete material class exhibiting high mechanical strength and ductility simultaneously is known as UHP-ECCs, also referred in the literature as high-strength high-ductility concrete. UHP-ECCs exhibit high compressive strength (i.e., at least ≥120 MPa), high tensile strength (i.e., ~10-20 MPa), and high flexural strength (i.e., ~15-30 MPa) *(3, 11, 43–46)*. UHP-ECCs also possess high tensile ductility (i.e., ~2 to 10%), and high energy absorption capacity during the strain hardening regime (which can reach up to 1500 kJ/m^3) *(11, 43–48)*. These exceptional mechanical properties are achieved through a densely packed homogenous cementitious matrix reinforced with high strength and high aspect ratio synthetic fibers instead of steel fibers, which are commonly used in UHPC. Furthermore, UHP-ECCs are optimized by tailoring matrix and fiber/matrix interfacial properties through carful mixture proportioning and basic ingredients selection. The type of synthetic fiber that has been successfully used in the design of UHP-ECC is ultra-high-molecular-weight (UHMW) polyethylene (PE) fiber, which possess a very high tensile strength and is hydrophobic. The excellent mechanical properties of the UHMW PE fiber is essential as this is needed to transfer the large interfacial frictional stresses produced by the densely packed UHP-ECC matrix without rupturing, thus allowing for the PSH strength criteria to be met. Moreover, the hydrophobic nature of UHMW PE fibers is also key as this eliminates the fiber/matrix interfacial chemical bond leading to a high complimentary energy of the fiber bridging relation, and consequently allowing for the PSH energy criteria to be met *(49)*. Table 2 present the properties of some of the UHMW PE fibers that have been utilized in the literature to produced UHP-ECC. As it can be observed, the aspect ratio and tensile strength of the UHMW PE fibers ranges between 450-900 and 2400-3800 MPa, respectively.

Table 2. Properties UHMW PE fibers utilized in high-strength high-ductility ECC

Authors	Diameter, D (um)	Length, L (mm)	Aspect Ratio (L/D)	Strength (MPa)
Yu et al. (2020) *(50)*	24	12	500	2400
	24	18	750	2400
	20	18	900	2800
Zhang et al. (2019)*(51)*	26	18	692	3000
Yu et al. (2018)*(3)*	20	18	900	3000
Yu et al. (2017)*(11)*	25	18	720	2900
	20	18	900	3800
Ranade et al. (2013)*(49)*	28	12.7	454	3000
Zhou et al. (2018) *(12)*	25	18	720	2900

4. METHODOLOGY

4.1. Materials

Type I ordinary Portland cement (OPC), silica fume (SF), Class F fly ash (FA), ordinary natural river sand (OS), microsilica sand (MS), high-range water-reducer (HRWR), potable water, and UHMW PE fiber were the components used in the production of the UHP-ECC materials evaluated in this research. All the components are readily available in the U.S., except for the UHMW PE fiber. Using X-ray fluorescence (XRF) spectroscopy analysis, the chemical structure of OPC and FA was determined, as shown in Table 3. The properties of SF (MasterLife SF 100, BASF), which were given by the producer are shown in Table 4. OPC, FA, SF, OS, and MS had specific gravities of 3.15, 2.29, 2.20, 2.61, and 2.65, respectively.

Table 3. OPC and FA chemical composition (weight %)

Material	SiO_2	Al_2O_3	Fe_2O_3	CaO	MgO	SO_3	K_2O	Na_2O
Cement	19.24	4.75	3.35	65.81	2.20	3.61	0.54	-
Fly Ash	62.08	18.56	8.22	5.69	1.69	0.37	1.42	0.35

Table 4. Silica fume properties

Silicon dioxide (SiO2), min, %	85.0
Chloride ions (CI), max, %	0.5
Sulfur trioxide (SO3), max, %	3.0
Available alkalies, as Na2O, max, %	1.5
Moisture content, max, %	3.0
Loss on ignition, max, %	6.0
Specific surface are (BET), min, m2/gm	15.0
Bulk density, lbs/cubic foot	30.0-50.0

A Beckman LS200 was used to determine the particle size distribution of OPC, FA, SF, OS, and MS determined as shown in Figure 3. In the case of SF, the particle size distribution was given by the producer. Table 5 shows the properties of the UHMW PE fiber (Qianxilong, China) used in the production of the UHP-ECC.

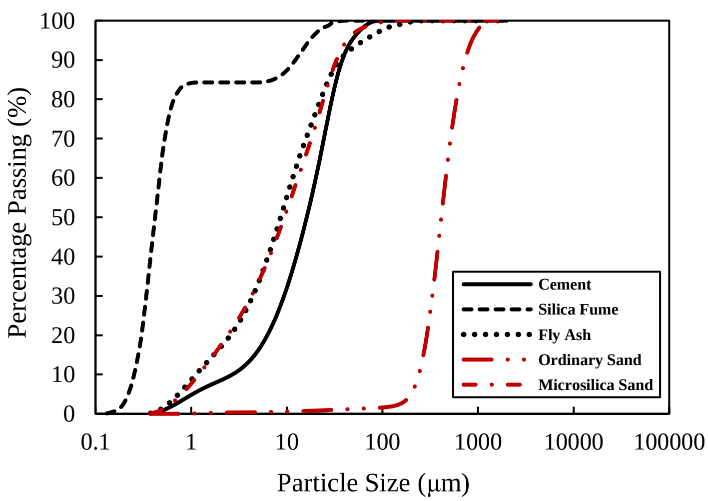

Figure 3. UHP-ECC components particle size distribution

Table 5. Properties of UHMW PE fiber

Fiber Type	Length (mm)	Diameter (μm)	Young's Modulus (GPa)	Tensile Strength (MPa)	Elongation (%)	Density (g/cm^3)
UHMW PE	12	15	145	3900	3.5	0.97

4.2. Mixture Proportions

4.2.1. Evaluation of Cementitious Matrices

Initially, an evaluation of the compositional factors affecting the compressive strength of cementitious matrices was conducted. This was performed in order to determine compositions exhibiting compressive strength equal to or greater than 120 MPa. Variables investigated included mass ratios of SF/FA, SCMs to cement (SCMs/C), and OS/MS. Table 6 present the variables and levels explored in this portion of the study. The water to binder ratio (W/B), and sand to binder ratio (S/B) were maintained at 0.24, 0.3, respectively. Furthermore, all cementitious matrices were reinforced with 1 vol.% UHMW PE fiber to prevent brittle failure of the specimens. The High-Range Water-Reduce (HRWR) was used at a constant content of 1.85% of the binder (by mass). A total of 36 cementitious matrices results from the variables and levels evaluated. Mixture proportions are shown in Table 7.

Table 6. Experimental variables and levels assessed

Variables	Levels	Description of Levels
SF/FA	4	0, 1/9, 1/4, and 3/7 (i.e., 0, 10, 20, and 30% replacement of FA with SF)
SCMs/C	3	4/6, 1, and 1.5 (i.e., 40, 50, and 60% replacement of C with SCMs)
OS/MS	3	0, 2/6, and 1 (i.e., 0, 25, and 50% replacement of OS with MS)

Table 7. Mixture proportions (kg/m3)

Mix ID	Cement	Silica Fume	Fly Ash	Water	River Sand	Microsilica Sand	Fibers (Vol%)
M1	826.9	0.0	551.3	330.8	0.0	413.4	1.0
M2	826.1	55.1	495.6	330.4	0.0	413.0	1.0
M3	825.2	110.0	440.1	330.1	0.0	412.6	1.0
M4	824.4	164.9	384.7	329.8	0.0	412.2	1.0
M5	826.4	0.0	550.9	328.3	105.6	309.9	1.0
M6	825.6	55.0	495.3	327.9	105.5	309.6	1.0
M7	824.7	110.0	439.9	327.6	105.4	309.3	1.0
M8	823.9	164.8	384.5	327.3	105.3	309.0	1.0
M9	825.9	0.0	550.6	325.8	211.1	206.5	1.0
M10	825.1	55.0	495.0	325.4	210.9	206.3	1.0
M11	824.3	109.9	439.6	325.1	210.7	206.1	1.0
M12	823.4	164.7	384.3	324.8	210.4	205.9	1.0
M13	677.8	0.0	677.8	325.4	0.0	406.7	1.0
M14	677.0	67.7	609.3	325.0	0.0	406.2	1.0
M15	676.2	135.2	540.9	324.6	0.0	405.7	1.0
M16	675.3	202.6	472.7	324.2	0.0	405.2	1.0
M17	677.4	0.0	677.4	322.9	103.9	304.8	1.0
M18	676.6	67.7	608.9	322.5	103.8	304.5	1.0
M19	675.8	135.2	540.6	322.1	103.6	304.1	1.0
M20	674.9	202.5	472.5	321.7	103.5	303.7	1.0

Mix ID	Cement	Silica Fume	Fly Ash	Water	River Sand	Microsilica Sand	Fibers (Vol%)
M21	677.0	0.0	677.0	320.4	207.6	203.1	1.0
M22	676.2	67.6	608.6	320.0	207.4	202.9	1.0
M23	675.4	135.1	540.3	319.7	207.1	202.6	1.0
M24	674.5	202.4	472.2	319.3	206.9	202.4	1.0
M25	533.5	0.0	800.3	320.1	0.0	400.2	1.0
M26	532.8	79.9	719.3	319.7	0.0	399.6	1.0
M27	532.0	159.6	638.4	319.2	0.0	399.0	1.0
M28	531.2	239.1	557.8	318.7	0.0	398.4	1.0
M29	533.2	0.0	799.9	317.7	102.2	299.9	1.0
M30	532.5	79.9	718.8	317.3	102.1	299.5	1.0
M31	531.7	159.5	638.0	316.8	101.9	299.1	1.0
M32	530.9	238.9	557.5	316.3	101.8	298.7	1.0
M33	532.9	0.0	799.4	315.3	204.3	199.8	1.0
M34	532.2	79.8	718.4	314.8	204.0	199.6	1.0
M35	531.4	159.4	637.7	314.4	203.7	199.3	1.0
M36	530.6	238.8	557.2	313.9	203.4	199.0	1.0

4.2.2. Evaluation of UHP-ECCs

Based on the findings from the evaluation of the cementitious matrices, two cementitious matrices were selected for the production of UHP-ECCs. Both cementitious matrices kept constant the S/B ratio, W/B ratio, and SCMs/C ratio at 0.36, 0.17, and 0.25 by mass, respectively. The only difference in the composition of the cementitious matrices was the SF/FA ratio. One cementitious matrix utilized a SF/FA ratio of 0.25, whereas the other one did not incorporated SF (i.e., SF/FA=0). Both cementitious matrices were reinforced with UHMW PE fiber at 1.5 and 2 vol.% yielding a total of four UHP-ECC compositions. Importantly, the HRWR was used at a constant content of 1.85% of the binder (by mass) for all mixtures. The mixture proportions of the UHP-ECC composites developed in this study are shown in Table 8. The mixture label format used was FA_xSF_y-f_z where x, y, and z stand for content of FA (by mass OPC), SF (by mass of OPC), fiber (vol.%)., respectively.

Table 8. Mixture proportions

Mix ID	Cement (kg/m^3)	Silica Fume (kg/m^3)	Fly Ash (kg/m^3)	Water (kg/m^3)	River Sand (kg/m^3)	Fiber (kg/m^3) [vol.%]
$FA_{20}SF_5$-$f_{1.5}$	1212.4	60.6	242.5	239.6	563.6	14.5 [1.5%]
$FA_{20}SF_5$-f_2	1206.2	60.3	241.2	238.4	560.8	19.4 [2%]
FA_{25}-$f_{1.5}$	1213.7	0.0	303.4	239.8	564.3	14.5 [1.5%]
FA_{25}-f_2	1207.6	0.0	301.9	238.6	561.4	19.4 [2%]

4.3. Material Preparation

A planetary mixer was implemented in the preparation of the cementitious matrices and UHP-ECCs. As a first step, the dry powders (OPC, FA, SF, OS) were mixed at 60 rpm (slow speed) for a minute. Second, both potable water and the HRWR were added and mixed for a minute at 60 rpm (slow speed), followed by an additional eleven minutes at 110 rpm (medium speed). Third, 50% of the UHMW PE fibers were added to the mix at 110 rpm (medium speed) and then mixed at 200 rpm (high speed) for an additional two minutes. Fourth, the remaining 50% of the fibers were added to the mix at 110 rpm (medium speed) and then mixed at 200 rpm (high speed) for an extra four minutes. Once the mixing process ended, the samples were cast and covered with a plastic sheet to limit moisture loss. Finally, the specimens were taken out of their moulds after 24 hours and subsequently cured in lime-saturated water for 28 days at ambient temperature, as per ASTM C511 *(52)*.

4.4. Testing Methods

4.4.1. Flow Table Test

To evaluate the workability of the composites, ASTM C1437 was implemented upon the completion of the mixing procedure as shown in Figure 4 *(53)*.

Figure 4. Flow table test

4.4.2. Compressive Strength Test

ASTM C109, was implemented to assess the compressive strength of cementitious matrices and UHP-ECCs *(54)*. This method was selected as it has been adopted in previous studies to evaluate UHP-ECCs' compressive strength *(49, 55, 56)*. For each mixture, a total of three cubes (50 mm x 50 mm x 50 mm) were cast and evaluated after curing for 28 days. Figure 5a shows the hydraulic pressure machine that was used to perform the test, using a steady 0.25 MPa/s loading rate. Cube specimens after test conclusion can be seen in Figure 5b.

(a) **(b)**

Figure 5. (a) test configuration, and (b) cube samples at test completion

4.4.3. *Uniaxial Tensile Test*

Based on the guidance of the Japan Society of Civil Engineers (JSCE) the tensile properties of the UHP-ECC composites were assessed by performing uniaxial tensile tests *(57)*. For each UHP-ECC mixture, six dumbbell specimens were cast, cured for 28 days, and then tested. The effective area dimensions of the dumbbell samples were 13 mm x 30 mm x 80 mm. A 0.5 mm/min loading rate was implemented and linear displacement sensors were used to measure the deformation of the central part of the dumbbell. The uniaxial test setup can be seen in Figure 6a. Figure 6b shows a dumbbell specimen at test completion. At the end of the test, the cracks on the specimens were analysed using an optical microscope. The images collected using the microscope were then processed using the software VIA Image Annotator, and subsequently the average crack width for each crack was obtained from the processed data file using Python. Finally, the average crack width for the specimen was obtained by averaging the crack widths for all individual cracks on the specimen.

(a) (b)

Figure 6. (a) UTT test configuration, and (b) dumbbell samples at test completion

4.4.4. *Single Crack Tensile Test*

The single crack tensile test (SCTT) was implemented on notched dumbbell samples to attain the fiber-bridging relation of the UHP-ECC materials and quantify relevant fiber-bridging properties, i.e., σ_0, δ_0, and J'_b *(58, 59)*. For each UHP-ECC mixture, five notched-dumbbell samples were cast, cured for 28 days, and tested. For the purpose of the SCTT a fiber content of 0.5 vol.% UHMWPE was used. This is customary in order to avoid the development of multiple cracks during the test, which prevent the accurate determination of $\sigma(\delta)$. The dimensions of the notched dumbbell specimens are displayed in Figure 7a. A 250 kN servo-hydraulic machine was used to perform the SCTT with a 0.5 mm/min loading rate. To measure the crack opening displacements of the specimens, linear displacement sensors were used. A gauge length of 20 mm was used for the test. When compared to the UTT, the gauge length is smaller in the SCTT to prevent the elastic deformation of the cementitious matrix to contribute to the resulting crack opening displacement. Dumbbell specimens after test completion can be seen in Figure 7b.

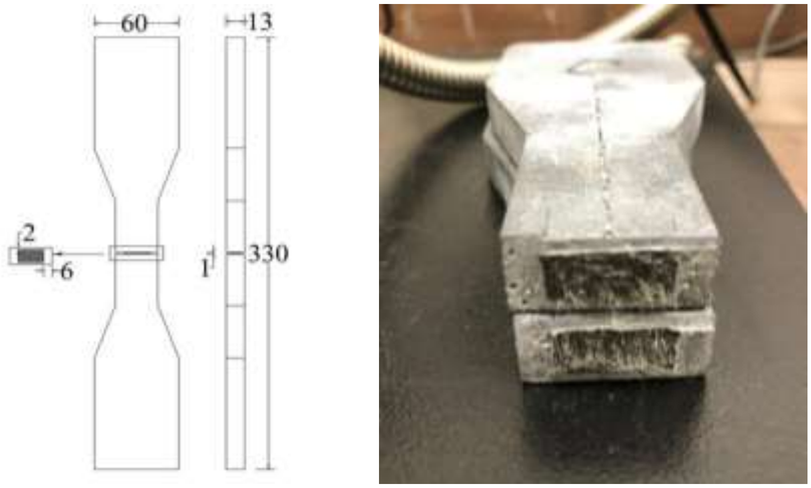

(a) (b)

Figure 7. (a) dumbbell sample dimensions with notch (Adapted from (16)), and (b) dumbbell specimen at test completion

4.4.5. Fracture Toughness Test

Three-point bending test were implemented on notch-beam samples for the two cementitious matrices (i.e., $FA_{20}SF_5$ and FA_{25}) assessed to determine relevant matrix properties, i.e., fracture toughness (K_m), crack tip fracture toughness (J_{tip}), and elastic modulus (E_m). For each UHP-ECC matrix mixture (i.e., with no fiber content), six notched-beam specimens were cast, cured for 28 days, and tested. The notched beam dimensions were 75 mm x 75 mm x 300 mm. A notch depth to beam depth ratio (a/d) of 0.5 and span to depth ratio (l/d) of 4 were used. As shown in Figure 8a, a universal testing system was implemented for the test, using a 0.18 mm/min loading rate. In order to attain the deformation at the middle of the notched-beam sample span, linear displacement sensors were used. Figure 8b shows a notched-beam sample after test completion. The effective crack model (ECM) was followed to determine K_m and E_m *(60, 61)*:

$$E_m = \frac{0.413P_i}{\delta_i}\left\{\frac{l^3\left(1+\frac{5wl}{8p_i}\right)}{4bd^3\left(1-\frac{a}{d}\right)^3} + \frac{1.17l}{1.68bd\left(1-\frac{a}{d}\right)}\right\} \quad (3)$$

Where:
δ_i = deflection corresponding to P_i,
b = beam width,
P_i = arbitrary load level,
d = beam depth,
l = beam span,
a = initial notch depth, and
w = self-weight of the specimen unit length

$$K_m = \sigma_n\sqrt{a_e}Y(\alpha) \quad (4)$$

Where:

$$M = \left(P_{max} + {}^{wl}/_{2}\right){}^{l}/_{4} \quad (5)$$

$$\sigma_n = {6M}/{(bd^2)} \tag{6}$$

a_e = effective notch depth

$Y(\alpha)$ = correction factor, determined as follows:

$$Y(\alpha) = \frac{1.99 - \alpha(1-\alpha)(2.15 - 3.93\alpha + 2.70\alpha^2)}{(1+2\alpha)(1-\alpha)^{1.5}} \tag{7}$$

with $\alpha = {a_e}/{d}$.

Lastly, J_{tip} is determined as follows:

$$J_{tip} = \frac{K_m^2}{E_m} \tag{8}$$

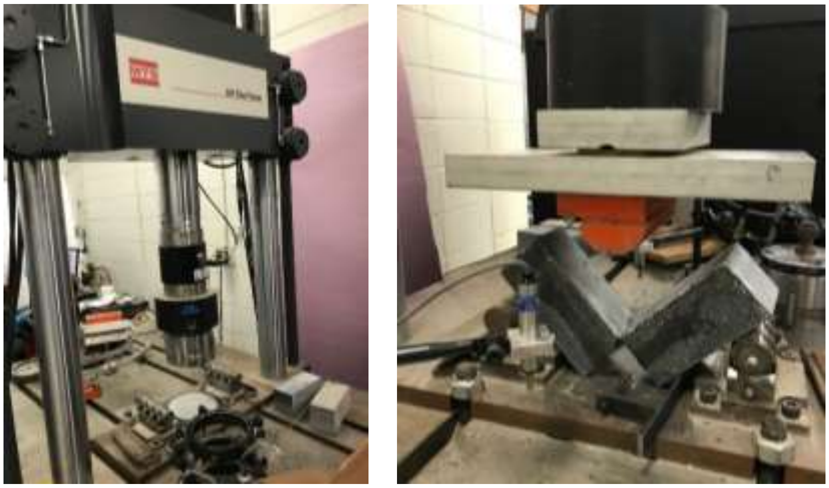

(a) (b)

Figure 8. (a)Universal testing system configuration (b)Notched-beam sample at test conclusion

4.4.6. Flexural Strength Test

Four-point bending test, according to ASTM C 1609, was implemented on 101.6 x 101.6 x 355.6 mm specimens to evaluate the flexural performance of the UHP-ECC composites assessed in this research*(62)*. For flexural loading, a span length of 300 mm and a 100 mm center span length were implemented. As shown in Figure 9a, a universal testing system was implemented for the test, using a 0.075 mm/min loading rate. In order to measure the deformation at the middle of the beam sample span, linear displacement sensors were used. Figure 9b shows beam samples at test completion.

(a) (b)

Figure 9. (a)Four-point bending test configuration (b)Beam samples at test conclusion

5. ANALYSIS AND FINDINGS

5.1. Cementitious Matrices

5.1.1. Compressive Strength

Table 9 displays the 28-day compressive strength for the 36 cementitious matrix mixtures considered in the first phase of this study. The 28-day compressive strength of the mixtures ranged from 50.2 to 99.5 MPa. As observed, the highest compressive strength was achieved by mixture M4. Mixture M4 corresponds to a FA/SF ratio of 3/7, a SCMs/C ratio of 4/6, and OS/MS ratio of 0. Generally, compressive strength results obtained were significantly higher than that of conventional concrete (i.e., 30 MPa) or high strength concrete (i.e., 55 MPa). However, the target compressive strength threshold of ≥120 MPa, to be considered a UHP-ECC, was not achieved.

Table 9. Compressive strength test results at 28 days

Mix ID	Average (MPa)	SD (MPa)	CV (%)
M1	77.8	1.5	2.0
M2	86.0	1.2	1.4
M3	89.9	3.2	3.5
M4	99.5	3.3	3.3
M5	86.4	1.2	1.4
M6	94.6	2.8	2.9
M7	96.9	7.7	8.0
M8	98.0	3.1	3.1
M9	88.1	1.5	1.7
M10	93.8	2.4	2.6
M11	91.0	6.1	6.7
M12	97.5	3.1	3.2
M13	80.0	1.9	2.3
M14	90.0	2.0	2.3
M15	88.8	3.9	4.4
M16	99.5	1.1	1.1
M17	82.0	1.8	2.2
M18	89.4	1.4	1.6
M19	86.7	3.3	3.8
M20	92.2	5.8	6.2
M21	77.3	1.3	1.7
M22	81.6	2.4	2.9
M23	79.7	1.8	2.3
M24	90.4	0.8	0.9
M25	72.1	0.9	1.2
M26	80.0	1.0	1.2
M27	87.3	0.4	0.5
M28	82.1	4.2	5.1
M29	98.2	4.3	4.4
M30	73.8	4.2	5.6
M31	83.9	2.5	3.0
M32	88.2	4.1	4.7
M33	50.2	3.9	7.7
M34	78.0	0.9	1.1
M35	80.7	1.3	1.6
M36	81.0	4.1	5.1

Linear regression models were created for each variable explored (i.e., SF/FA, SCMs/C, and OS/MS) to be able to understand their individual impact on the cementitious matrices' compressive strength. Equations 7, 8, and 9 present the regression models for SF/FA, SCMs/C, and OS/MS, respectively. The coefficient of determination (R^2) for the regressions presented in equations 7, 8, and 9 were 0.21, 0.25, and 0.04, respectively.

$$f'c = 27.92 \frac{SF}{FA} + 80.40 \quad (9)$$

$$f'c = -14.40 \frac{SCMs}{C} + 101.12 \quad (10)$$

$$f'c = -4.58 \frac{OS}{MS} + 87.94 \quad (11)$$

The SF/FA model indicated that higher SF/FA ratio values led to higher cementitious matrices' compressive strength. This can be credited to the fine particle size and high reactivity of SF when compared to FA, which may enhance the microstructure and particle packing density of the cementitious matrix resulting in increases in strength *(63)*. On the other hand, the resulting regression model for the SCMs/C ratio showed a worsening strength as the ratio increased. This can be attributed to the fact that the compression tests were performed at 28 days, time at which the pozzolanic reaction of the SCMs had not yet significantly affected compressive strength development *(64)*. It is foreseen that the effect of SCMs will increase the strength of the mixtures at later ages. Finally, the resulting linear regression for the OS/MS ratio displayed a small slope, implying that the OS/MS ratio had no significant effect in the strength development of the cementitious matrices. It is relevant to mention that although tendencies shown by the linear regressions are useful for understanding the results, the R^2 values obtained were very low.

A multiple linear regression model was developed to assess the impact of all the variables simultaneously on the cementitious matrices' compressive strength. The multiple linear regression results showed that the model was statistically significant (p-value <0.0001) and that resulting coefficients for each independent variable were also statistically significant (p-values <0.0001 for SF/FA and SCMs/C, and p-value of 0.0063 for OS/MS). Moreover, the R^2 was equal to 0.49, which is considerably greater than that of the linear regression models for individual variables. The multiple linear regression is presented in equation 10 below.

$$f'c = 27.92 \frac{SF}{FA} - 14.40 \frac{SCMs}{C} - 4.58 \frac{OS}{MS} + 97.64 \quad (12)$$

The multiple linear regression model shows the following trends: (1) SF/FA ratio had the biggest effect on strength, increasing it as the ratio increased; (2) a higher SCMs/C ratio results in worsening of the strength; (3) OS/MS ratio had the least effect on strength development, with a slight negative effect. By using equation 10, the compressive strength of the different mixtures evaluated was calculated (i.e., predicted strength) and compared to those obtained experimentally (i.e., actual strength) as shown in Figure 10. It can be appreciated that the model fairly determines the compressive strength values of the mixtures exhibiting strengths higher than approximately 75 MPa.

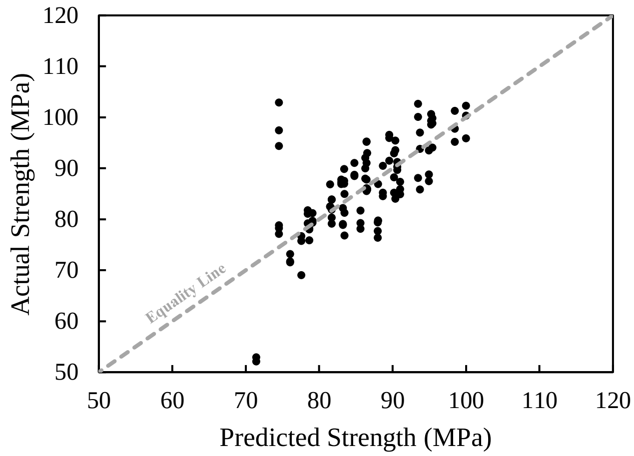

Figure 10. Actual vs. predicted compressive strength plot

Based on the results, it was noticed that cementitious matrices with higher SF/FA ratio and lower SCMs/C ratio should be evaluated to reach compressive strength values ≥120 MPa. In addition, the use of lower W/B ratios may also be necessary to achieve the target strength. Moreover, given the low effect on strength of the OS/MS variable, it was determined that OS can be utilized as the only fine aggregate to reduce the mixture costs and make them more practical. In the following phase this knowledge is implemented for the development of UHP-ECCs.

5.2. UHP-ECCs

Based on the knowledge obtained from the previous phase of the research, two cementitious matrices were developed to produce the UHP-ECCs. Relative to the cementitious matrices produced in the previous phase, the present cementitious matrices reduced the W/B from 0.24 to 0.17. Moreover, a low SCMs/C ratio (i.e., 0.25) was used, which was lower than the lowest level previously evaluated (i.e., 0.67). The sole difference between the two new cementitious matrices developed was the use of two different SF/FA ratios (i.e., 0 and 0.25) to evaluate the effect of moderate SF content and no SF on the properties of the mixtures. The two cementitious matrices were reinforced with UHMW PE fiber at two different vol.% (i.e., 1.5 and 2%), resulting in a total of four UHP-ECC mixtures as presented in Table 10.

5.2.1. Flow Table Test

The resulting spread diameters from the flowability test are shown in Table 10. Two clear trends were detected (1) a higher vol.% fiber content resulted in a decrease in flowability, and (2) using SF decreased the flowability of the mix. The decrease in flowability of the mix when using SF was attributed to the high surface area of SF, which increases water demand.

Table 10. Spread diameter (mm)

Mix	1	2	3	4	Avg.	SD	CV (%)	% Increase
$FA_{20}SF_5$-$f_{1.5}$	160.69	176.74	162.05	160.36	165.0	7.9	4.8	65.0%
$FA_{20}SF_5$-f_2	157.93	158.12	151.21	159.75	156.8	3.8	2.4	56.8%
FA_{25}-$f_{1.5}$	176.24	178.62	181.73	172.22	177.2	4.0	2.3	77.2%
FA_{25}-f_2	175.12	169.34	167.81	165.19	169.4	4.2	2.5	69.4%

5.2.2. *Compressive Strength Test*

Table 11 displays the compressive strength test results of the mixtures assessed in this study. From the results it can be noticed that the minimum compressive strength of 120 MPa was achieved by all mixtures, excluding $FA_{20}SF_5$-$f_{1.5}$. Furthermore, the highest compressive strength achieved was 133.1 MPa, for mixture FA_{25}-$f_{1.5}$. Intriguingly, the inclusion of SF in the mixtures resulted in a slight worsening of the compressive strength. This could be associated to the reduced workability of mixtures implementing SF, which may have allowed for the incorporation of more air bubbles. This hypothesis is supported by the inferior densities displayed for mixtures using SF as shown in Table 12. Concerning the impact on the compressive strength due to fiber content, there was no obvious trend. Mixtures including SF showed a minor increase in strength as the fiber content increased, while mixtures with no SF showed the contrary. An analysis of variance (ANOVA) was conducted at a 5% significance level. From the statistical analysis, it was encountered that differences observed in average compressive strength were not statistically significant (p-value=0.12). In turn, this suggests the necessity of an expanded dataset to elucidate whether the tendencies observed are real and not the construct of experimental variability.

Table 11. Compressive strength test results

Mix ID	1	2	3	Avg.	SD	CV (%)
$FA_{20}SF_5$-$f_{1.5}$	104.1	120.3	123.0	115.8	10.2	8.8
$FA_{20}SF_5$-f_2	124.8	124.1	131.0	126.6	3.8	3.0
FA_{25}-$f_{1.5}$	129.3	135.2	134.7	133.1	3.2	2.4
FA_{25}-f_2	138.0	131.9	117.1	129.0	10.8	8.3

Table 12. Hardened density (kg/m3)

Mix ID	1	2	3	Avg.	SD	CV (%)
$FA_{20}SF_5$-$f_{1.5}$	2262.0	2246.4	2245.7	2251.4	9.3	0.4
$FA_{20}SF_5$-f_2	2263.0	2263.4	2292.1	2272.9	16.7	0.7
FA_{25}-$f_{1.5}$	2319.0	2312.2	2313.1	2314.8	3.7	0.2
FA_{25}-f_2	2353.6	2364.9	2305.7	2341.4	31.5	1.3

5.2.3. *Single Crack Tensile Test*

Using the SCTT results for the two cementitious matrices with 0.5 vol.% UHMW PE fiber, the fiber-bridging relation curves for 1.5 and 2 vol.% fiber contents were calculated and plotted with the help of scaling factors (as shown in Figure 11). A small fiber content (i.e., 0.5% vol.%) was used in the test to prevent multiple-cracking behaviour, which is prone to occur with these materials. Previous research has discussed the implementation of scaling factors in the prediction of $\sigma(\delta)$ for different fiber contents *(7)*.

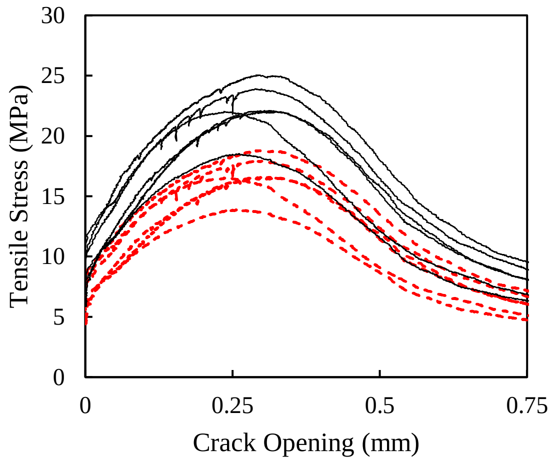

(a)

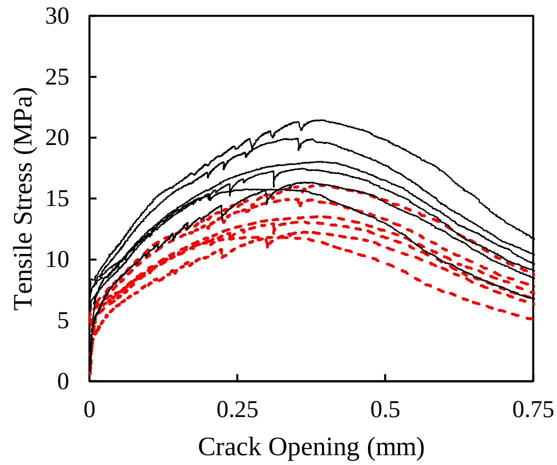

(b)

Figure 11. Fiber-bridging relation curves: (a) FA20SF5-f1.5 (dashed) and FA20SF5-f2 (solid), (b) FA25-f1.5 (dashed) and FA25-f2 (solid)

From the fiber-bridging relationships presented in Figures 11a and 11b, fundamental fiber-bridging properties were determined including σ_0, δ_0, and J'_b. These properties are shown in Table 13. From the results it can be noticed that utilizing SF increased σ_0 but decreased δ_0. This may be associated to an enhancement in the interface frictional bond (τ_0) between the fiber and the cementitious matrix, as a result of a dense microstructure improved by the fine particle size and reactivity of SF *(65–67)*. Although the use of SF enhanced σ_0, due to the marked decrease in δ_0, J'_b decreased. In turn, the decrease in J'_b is disadvantageous when trying to obtain PSH behavior. Importantly, a higher fiber content resulted in higher values of σ_0 and J'_b, which makes augmenting the fiber content appealing to achieve materials with enhanced tensile strength and ductility. However, the increase in fiber content can result in fiber dispersion problems, which can limit improvements in fiber-bridging properties. Moreover, increasing fiber content substantially increases the cost of the composites. It is relevant to mention that the properties shown in Table 13 assume adequate fiber dispersion and an insignificant effect of the fiber content increase on the characteristics of the cementitious matrix. This is the case since tests were conducted at a fiber content of 0.5 vol.%.

Table 13. Fiber bridging properties: σ_0, δ_0, and J'_b

Properties	$FA_{20}SF_5$-$f_{1.5}$		$FA_{20}SF_5$-f_2		FA_{25}-$f_{1.5}$		FA_{25}-f_2	
	Avg.	**SD**	**Avg.**	**SD**	**Avg.**	**SD**	**Avg.**	**SD**
σ_0 (MPa)	16.7	1.7	22.3	2.2	13.6	1.6	18.2	2.2
δ_0 (mm)	0.28	0.03	0.28	0.03	0.36	0.03	0.36	0.03
J'_b (J/m^2)	688.9	400.7	918.5	534.3	909.4	181.0	1212.5	241.3

5.2.4. Fracture Toughness Test

The results from the fracture toughness test for both cementitious matrices considered are shown in Table 14. Resulting J_{tip} values indicate that utilizing SF in the mixture had an apparent worsening effect. In turn, this would imply that in terms of matrix properties, cementitious matrices including SF are more conducive for PSH behaviour. Notwithstanding, a t-test conducted at a 5% significance level revealed that the difference in average J_{tip} was not statistically significant (p-value=0.86). As such, further testing is warranted to make a definite determination.

Table 14. Matrix crack tip fracture toughness J_{tip} (J/m2)

Mix ID	1	2	3	Avg.	SD	CV (%)
$FA_{20}SF_5$	39.6	43.5	25.2	36.1	9.7	26.8
FA_{25}	73.8	90.3	23.2	62.4	35.0	56.0

5.2.5. Uniaxial Tensile Test

From the tensile stress vs. strain curves shown in Figure 12, the tensile strength (σ_u), matrix cracking strength (σ_{cr}), and tensile strain capacity (ε_u) of the composites were determined and summarized in Table 15. In addition, to better understand the tensile performance of the UHP-ECC materials, the energy and strength PSH indexes were calculated from the previously attained fiber-bridging and cementitious matrix properties σ_0, J'_b, J_{tip}, and σ_c, as shown in Table 16.

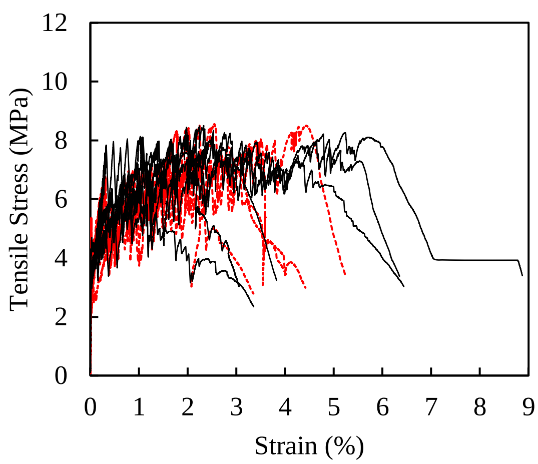

(a)

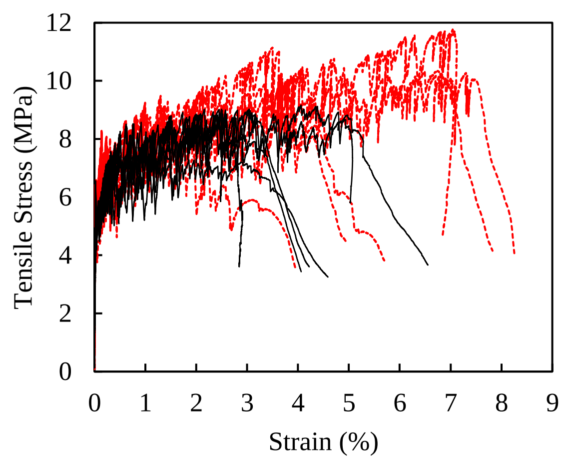

(b)

Figure 12. Tensile stress vs. strain curves: (a) FA20SF5-f1.5 (dashed) and FA20SF5-f2 (solid), (b) FA25-f1.5 (dashed) and FA25-f2 (solid)

Table 15. Tensile strength, cracking strength, and tensile strain capacity

Properties	$FA_{20}SF_5$-$f_{1.5}$		$FA_{20}SF_5$-f_2		FA_{25}-$f_{1.5}$		FA_{25}-f_2	
	Avg.	SD	Avg.	SD	Avg.	SD	Avg.	SD
Tensile Strength (MPa)	7.74	0.64	7.68	0.98	10.33	1.04	8.79	0.38
Tensile Strain Capacity (%)	2.52	1.44	2.17	0.65	4.33	2.43	2.34	1.08
Cracking Strength (MPa)	4.24	1.11	3.81	0.58	5.25	0.85	5.16	0.83

Table 16. PSH strength and energy indexes

Properties	$FA_{20}SF_5$-$f_{1.5}$	$FA_{20}SF_5$-f_2	FA_{25}-$f_{1.5}$	FA_{25}-f_2
σ_0(MPa)	16.7	22.3	13.6	18.2
σ_{cr} (MPa)	4.2	3.8	5.2	5.2
PSH Strength Index	3.9	5.8	2.6	3.5
J'_b (J/m^2)	688.9	918.5	909.4	1212.5
J_{tip} (J/m^2)	36.1	36.1	48.5	48.5
PSH Energy Index	19.1	25.4	18.8	25.0

From the tensile properties reported in Table 15, it can be observed that all the composites exhibited ECC-like ductility (i.e., >2% tensile strain capacity). Accordingly, the remarkable ductility of the materials is supported by the PSH strength and energy indexes obtained, which far exceeded the minimum values desire for robust PSH behavior of 1.3 and 2.7, respectively (see Figure 13). Furthermore, the following tendencies were observed: (1) the use of SF had a negative effect in the tensile strength and strain capacity of the composites; and (2) incrementing the vol.% fiber content produced no meaningful effect or a negative impact in the tensile strength and strain capacity of the materials. From the fiber-bridging capacities reported in Table 16, it is predicted that both the use of SF and augmenting the fiber content should enhance the tensile strength of the composites. Moreover, from the PSH indexes (see Figure 13) it is expected that augmenting the fiber content produces substantial improvements in the material's PSH behavior and thus in their tensile ductility. Nonetheless, the opposite tendencies were observed. However, a reasonable justification exists for the phenomena observed. To attain $\sigma(\delta)$ at 1.5 and 2% fiber content, scaling factors were used from 0.5% fiber content curves. However, for the use scaling factors to be accurate, the increase in fiber content should not significantly affect the fiber distribution or the fiber/matrix interface properties. From the results, it is believed that augmenting the fiber content from 0.5% to 1.5 and 2% negatively affected fiber distribution. This is the case as a significant workability loss was detected when augmenting the fiber content from 0.5% to 1.5% and 2%, thus producing the possibility of fiber clumping. In fact, some fiber clumps were detected in fresh mixtures implementing 2% fiber content (by visual inspection and touch), especially for mixtures implementing SF. As such, values of σ_0 and J'_b obtained for mixtures using 1.5 and 2% fiber content were likely overestimated, especially for materials using 2% fiber content. It is relevant to notice that the sand utilized in this study (i.e., natural river sand) is significantly coarser than the sand conventionally used in the development of ECCs or UHP-ECCs (i.e., manufactured microsilica sand), which may intensify fiber distribution issues. This can happen given that the use of sand with a particle size superior than the average space between the fibers, can result in increased interaction between the aggregate and the fiber, contributing to fiber clumping *(68, 69)*. Table 15 also shows that the matrix cracking strength decreased as fiber content incremented and SF was used. In turn, this could be indicative of worsening fiber dispersion given that fiber clumps can behave as defects in the composites and negatively impact the matrix cracking strength.

An ANOVA (at 5% significance level) was conducted to examine the statistical significance of the findings. From the ANOVA, statistically significant differences were encountered in the average tensile strength (p-value<0.0001) and matrix first-cracking strength (p-value=0.022) of the composites. Nonetheless, the differences in average tensile strain capacity of the UHP-ECCs were not statistically significant (p-value=0.087), thus warranting further evaluation to confirm tendencies observed in tensile ductility. Tukey-Kramer Honestly Significant Difference (HSD) tests were conducted for the tensile strength and matrix first-cracking strength to determine statistically significant differences among the materials evaluated. From the analysis, it was determined that the difference in tensile strength of mixture FA_{25}-$f_{1.5}$ in contrast to all other mixtures was statistically significant. In turn, this finding suggests that (1) the decrease in tensile strength when using SF is significant at 1.5% fiber content, and (2) the decrease in tensile strength when increasing the amount of fiber from 1.5 to 2% for composites with no SF was significant. In the case of the first-cracking strength, a statistically significant difference was only encountered between $FA_{20}SF_5$-f_2 and FA_{25}-$f_{1.5}$. Consequently, this tells us that the combined effect of implementing SF and augmenting fiber content from 1.5 to 2% produced a significant decrease in the matrix first-cracking strength. This supports the hypothesis using SF and the increase in fiber content led to fiber agglomeration, which acted as defects in the material, thus negatively affecting the composite's fiber-bridging and matrix properties.

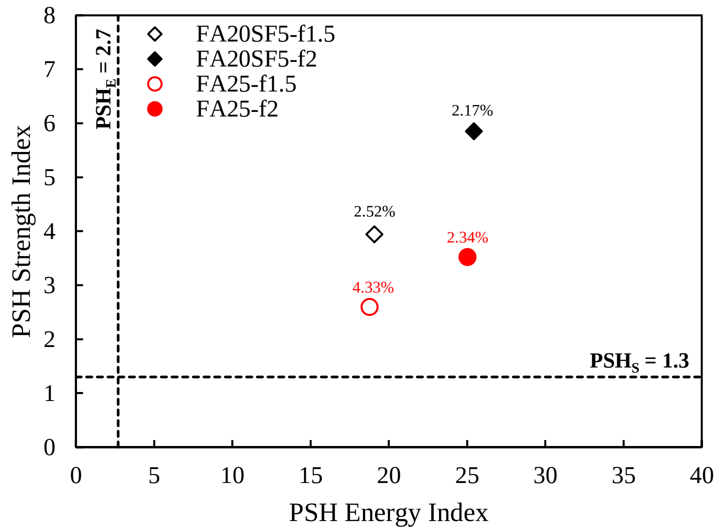

Figure 13. PSH indexes and corresponding tensile strain capacities of the composites

It is important to point out that mixture FA_{25}-$f_{1.5}$, which used readily available components and a relatively low fiber content (1.5%), presented remarkable compressive strength (133.1 MPa), tensile strength (10.3 MPa), and tensile strain capacity (4.3%). Importantly, SF and MS were not used in mixture FA_{25}-$f_{1.5}$. This is significant as these ingredients are seldom left out in the production of UHP-ECC and contribute to a significant increment in price, loss of workability and reduced practicality of the composites.

5.2.6. Flexural Performance Test

The flexural performance results for all UHP-ECC mixtures considered are shown in Table 17. Figure 14 shows the flexural tensile stress vs. deflection curves. It can be observed that all mixtures assessed displayed deflection hardening behavior after reaching the first-cracking strength. This behavior was foreseen since flexural performance of concrete composites is governed by its tensile performance. Thus, the previously discussed tensile behavior could be seen reflected on the flexural performance of the beam samples. Furthermore, fluctuations in mixture composition had a similar effect on the strength and ductility of the materials to those observed during the tensile test. Nonetheless, using ANOVA, no statistically significant differences were obtained for the first-cracking strength (p-value=0.56), flexural strength (p-value=0.28), and deflection capacity (p-value=0.12). It is important to mention that the highest average first-cracking strength was obtained by mixture FA_{25}-$f_{1.5}$, while the highest average flexural strength and deflection capacity were obtained by FA_{25}-f_2.

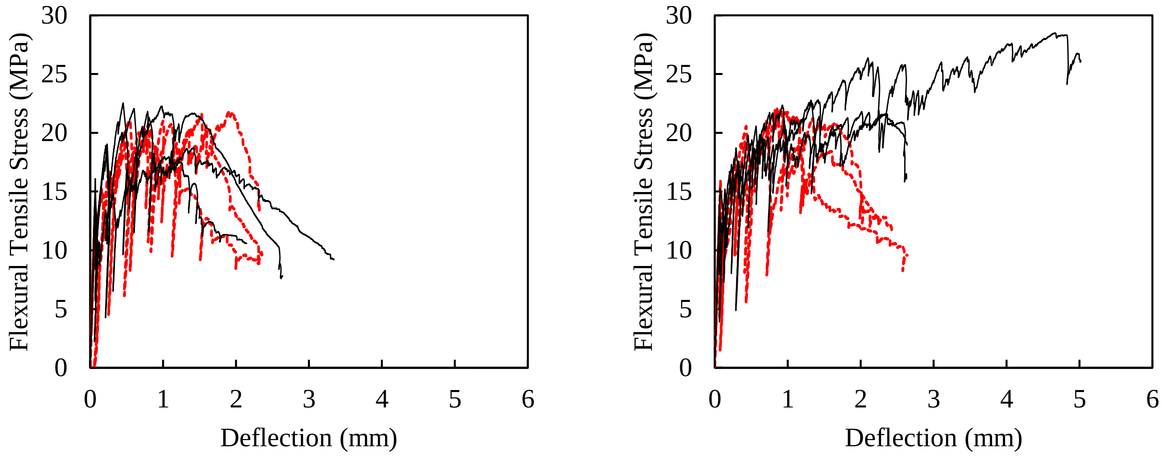

(a) **(b)**

Figure 14. Flexural tensile stress vs. deflection curves: (a) FA20SF5-f1.5 (dashed) and FA20SF5-f2 (solid), (b) FA25-f1.5 (dashed) and FA25-f2 (solid)

Table 17. Flexural performance properties: first cracking strength, flexural strength, and deflection capacity

Properties	$FA_{20}SF_5$-$f_{1.5}$		$FA_{20}SF_5$-f_2		FA_{25}-$f_{1.5}$		FA_{25}-f_2	
	Average	**SD**	**Average**	**SD**	**Average**	**SD**	**Average**	**SD**
First-Cracking Strength (MPa)	12.94	0.80	14.00	2.02	14.43	1.06	14.12	1.03
Flexural Strength (MPa)	21.26	0.40	20.85	2.52	21.44	0.85	24.36	3.62
Deflection Capacity (mm)	1.15	0.69	0.71	0.33	0.87	0.14	2.67	1.77

5.2.7. Crack Analysis

Table 18 displays the average crack width and average number of cracks obtained from the dumbbell specimens after the uniaxial tensile test. As can be observed from Table 18, the average crack width for the specimens was in the range of 61 μm to 131 μm, while the average number of cracks ranged from 18.2 to 31.0. The average crack widths obtained are well within the range of 50 μm to 180 μm mentioned in the literature for UHP-ECCs. Also, Table 18 shows that the implementation of SF in the mixtures resulted in a smaller number of cracks, which in turn negatively affects tensile ductility. Mixtures with no SF also displayed a better tensile strain capacity in the uniaxial tensile test, which concurs with results attained in this section.

Table 18. Crack analysis: average crack width and average number of cracks

Properties	$FA_{20}SF_5$-$f_{1.5}$		$FA_{20}SF_5$-f_2		FA_{25}-$f_{1.5}$		FA_{25}-f_2	
	Average	**SD**	**Average**	**SD**	**Average**	**SD**	**Average**	**SD**
Average Crack Width (μm)	110.1	29.1	131.0	17.0	115.3	16.8	61.5	12.6
Average Number of Cracks	18.2	6.7	23.8	8.6	31.0	10.0	26.0	7.0

6. CONCLUSIONS

The aim of this research study was to produce novel UHP-ECC materials utilizing readily available ingredients for the construction and repair of transportation infrastructure in Region 6. The first phase of the study focused on the evaluation of the effect of ingredient selection and mixture proportioning on the cementitious matrices' mechanical strength for the production of UHP-ECCs. Variables evaluated included the mass ratios of SF/FA, SCMs/C, and OS/MS. Subsequently, the second phase of the study adopted the knowledge obtained in the first phase to develop of UHP-ECCs. In the development of UHP-ECCs, the effect of silica fume on the composite's fiber-bridging and matrix properties were assessed. Furthermore, the effect of silica fume and fiber content on the composite's fresh and hardened properties were evaluated. From the experimental results the following conclusions can be inferred:

- The mass ratio of SF/FA had the most relevant effect on the cementitious matrices' compressive strength, followed by the SCMs/C ratio, and finally the OS/MS ratio. Furthermore, generally, the effects of the SF/FA, SCMs/C, and OS/MS ratios on the matrices' compressive strength were as follows: (1) increments in SF/FA produced improvements in strength, (2) increments in SCMs/C produce decrements in strength, and (3) increments in the OS/MS produced slight decrements in strength. A multiple linear regression model was developed to predict the compressive strength of cementitious matrices from the variables evaluated.

- The incorporation of SF produced a decrease in workability of the fresh UHP-ECC mixtures. Furthermore, augmenting fiber content from 1.5 to 2 vol.% did also worsen the workability of the UHP-ECCs. Fiber clumps were detected by visual inspection and touch on mixtures implementing 2 vol.% fiber content.

- Excepting mixture $FA_{20}SF_5$-$f_{1.5}$, all the composites produced presented compressive strengths greater than 120 MPa. Moreover, the compressive strength of the composites ranged from 115.8 to 133.1 MPa. While augmenting fiber content from 1.5 to 2 vol.% did not produce any obvious trend in the compressive strength, the implementation of SF in the composites produced an apparent decrease in strength. The decrease in strength with SF was accompanied by the decrease in hardened density, which was attributed to the inclusion of additional entrapped air given the decrease in workability caused by SF. Nonetheless, statistically significant differences in the compressive strength of the materials were not found.

- The incorporation of SF increased σ_0, yet it decreased δ_0 leading to a decrease of J'_b. In turn, in terms of fiber-bridging properties the use of SF is not advantageous to promote the PSH behavior of the composites; however, it is conducive to increasing the tensile strength. In the case of matrix properties, the use of SF produced an apparent decrease in J_{tip}, which is beneficial for PSH response; nonetheless, the difference was not statistically significant. PSH indexes computed from matrix and fiber-bridging properties indicated that the use of SF does not meaningfully impact the PSH energy index, yet it increases the PSH strength index. Using scaling factors, fiber-bridging relations for 1.5 and 2 vol.% were obtained from the 0.5 vol.% curves experimentally determined. PSH indexes computed for 1.5 and 2 vol.% far exceeded the minimum recommended values for robust PSH behavior.

- All the composites produced presented ECC-like ductility (i.e., >2% tensile strain capacity) as predicted by the PSH indexes. Furthermore, the implementation of SF and augmenting the fiber content generally produced adverse impacts in the tensile strength and strain capacity of the composites. Notwithstanding, the tensile strain capacity differences were not statistically significant. While the tendencies observed contradicted the expected composite response, the observed results were attributed to a worsening fiber dispersion as SF was implemented and/or fiber content increased.

- Flexural performance test results revealed a deflection hardening response for all the composites developed. Furthermore, similar tendencies as those observed in the uniaxial tensile test results in terms of strength and ductility were observed. Nonetheless, no statistically significant differences were encountered for the flexural properties. Flexural strength of the composites ranged from 20.9 to 24.4 MPa, which is approximately 4 to 5 times that of conventional concrete.

- The average crack width for all materials was in the range of 61 μm to 131 μm, while the average number of cracks ranged from 18.2 to 31.0. Implementation of SF in the mixtures resulted in a smaller number of cracks, which concurs with the attained tensile strain capacity from the uniaxial tensile test.

As shown in Table 20 below, from the experimental results, the development of UHP-ECCs utilizing readily available ingredients was successfully achieved. Specifically, mixtures FA_{25}-$f_{1.5}$, FA_{25}-f_2, and $FA_{20}SF_5$-f_2 met the necessary requirements to classify as UHP-ECCs, i.e., simultaneously achieving ultra-high compressive strength (>120 MPa) and high tensile ductility (tensile strain capacity >2%). Importantly, mixture FA_{25}-$f_{1.5}$, which did not incorporate SF and used relatively low fiber content, displayed a compressive strength of 133.1 MPa (i.e., ~4.5 times that of concrete), tensile strength of 10.3 MPa (~3 times that of concrete), tensile strain capacity of 4.3% (~430 times that of concrete), and flexural strength of 21.4 MPa (~4 times that of concrete).

Table 20. Properties of UHP-ECCs (standard deviation presented in brackets)

Mixture ID	f'_c (MPa)[a]	MOR (MPa)[b]	σ_{cr} (MPa)[c]	σ_u (MPa)[d]	ε_u (%)[e]
$FA_{20}SF_5$-$f_{1.5}$	115.8 [10.2]	21.3 [0.4]	4.2 [1.1]	7.7 [0.6]	2.5 [1.4]
$FA_{20}SF_5$-f_2	126.6 [3.8]	20.9 [2.5]	3.8 [0.6]	7.7 [1.0]	2.2 [0.7]
FA_{25}-$f_{1.5}$	133.1 [3.2]	21.4 [0.9]	5.3 [0.9]	10.3 [1.0]	4.3 [2.4]
FA_{25}-f_2	129.0 [10.8]	24.4 [3.6]	5.2 [0.8]	8.8 [0.4]	2.3 [1.1]

[a] Compressive strength; [b] modulus of rupture (i.e., flexural strength); [c] matrix cracking strength; [d] tensile strength; [e] tensile strain capacity

7. REFERENCES

1. Ultra-High Performance Concrete. https://www.cement.org/learn/concrete-technology/concrete-design-production/ultra-high-performance-concrete. Accessed Feb. 5, 2021.

2. Standard Practice for Fabricating and Testing Specimens of Ultra-High Performance Concrete 1.

3. Yu, K. Q., J. T. Yu, J. G. Dai, Z. D. Lu, and S. P. Shah. Development of ultra-high performance engineered cementitious composites using polyethylene (PE) fibers. *Construction and Building Materials*, Vol. 158, 2018, pp. 217–227.

4. Larsen, I. L., and R. T. Thorstensen. The influence of steel fibres on compressive and tensile strength of ultra high performance concrete: A review. *Construction and Building Materials*, Vol. 256, 2020, p. 119459.

5. Wille, K., S. El-Tawil, and A. E. Naaman. Properties of strain hardening ultra high performance fiber reinforced concrete (UHP-FRC) under direct tensile loading. *Cement and Concrete Composites*, Vol. 48, 2014, pp. 53–66.

6. Amador, G. A., T. Rupnow, and M. Hassan. Evaluation of the Performance and Cost-Effectiveness of Engineered Cementitious Composites (ECC) Produced from Region 6 Local Materials. *Publications*, 2018.

7. Li, V. C. *Engineered Cementitious Composites (ECC) Bendable Concrete for Sustainable and Resilient Infrastructure*. Springer, 2019.

8. Li, V. C. *Engineered Cementitious Composites (ECC) – Material, Structural, and Durability Performance*. 2008.

9. Şahmaran, M., and V. C. Li. Engineered Cementitious Composites: Can Composites Be Accepted as Crack-Free Concrete? *https://doi.org/10.3141/2164-01*, No. 2164, 2010, pp. 1–8.

10. Liu, H., Q. Zhang, V. Li, H. Su, and C. Gu. Durability study on engineered cementitious composites (ECC) under sulfate and chloride environment. *Construction and Building Materials*, Vol. 133, 2017, pp. 171–181.

11. Yu, K., Y. Wang, J. Yu, and S. Xu. A strain-hardening cementitious composites with the tensile capacity up to 8%. *Construction and Building Materials*, Vol. 137, 2017, pp. 410–419.

12. Zhou, Y., B. Xi, K. Yu, L. Sui, and F. Xing. Mechanical Properties of Hybrid Ultra-High Performance Engineered Cementitous Composites Incorporating Steel and Polyethylene Fibers. *Materials*, Vol. 11, No. 8, 2018, p. 1448.

13. Hassan, A. M. T., S. W. Jones, and G. H. Mahmud. Experimental test methods to determine the uniaxial tensile and compressive behaviour of ultra high performance fibre reinforced concrete (UHPFRC). *Construction and Building Materials*, Vol. 37, 2012, pp. 874–882.

14. Kim, D. J., K. Wille, A. E. Naaman, and S. El-Tawil. Strength dependent tensile behavior

of strain hardening fiber reinforced concrete. In *High Performance Fiber Reinforced Cement Composites 6*, Springer, pp. 3–10.

15. Aghdasi, P., A. E. Heid, and S.-H. Chao. Developing Ultra-High-Performance Fiber-Reinforced Concrete for Large-Scale Structural Applications. *ACI Materials Journal*, Vol. 113, No. 5, 2016, pp. 559–570.

16. Wille, K., D. J. Kim, and A. E. Naaman. Strain-hardening UHP-FRC with low fiber contents. *Materials and Structures/Materiaux et Constructions*, Vol. 44, No. 3, 2011, pp. 583–598.

17. Park, S. H., D. J. Kim, G. S. Ryu, and K. T. Koh. Tensile behavior of ultra high performance hybrid fiber reinforced concrete. *Cement and Concrete Composites*, Vol. 34, No. 2, 2012, pp. 172–184.

18. Shi, C., Z. Wu, J. Xiao, D. Wang, Z. Huang, and Z. Fang. A review on ultra high performance concrete: Part I. Raw materials and mixture design. *Construction and Building Materials*, Vol. 101, 2015, pp. 741–751.

19. Park, C. K., M. H. Noh, and T. H. Park. Rheological properties of cementitious materials containing mineral admixtures. *Cement and Concrete Research*, Vol. 35, No. 5, 2005, pp. 842–849.

20. Yu, R., P. Spiesz, and H. J. H. Brouwers. Mix design and properties assessment of Ultra-High Performance Fibre Reinforced Concrete (UHPFRC). *Cement and Concrete Research*, Vol. 56, 2014, pp. 29–39.

21. Dils, J., G. De Schutter, and V. Boel. Influence of mixing procedure and mixer type on fresh and hardened properties of concrete: A review. *Materials and Structures/Materiaux et Constructions*, Vol. 45, No. 11, 2012, pp. 1673–1683.

22. Aïm, R. Ben, and P. Le Goff. Effet de paroi dans les empilements désordonnés de sphères et application à la porosité de mélanges binaires. *Powder Technology*, Vol. 1, No. 5, 1968, pp. 281–290.

23. De Larrard, F., and T. Sedran. Mixture-proportioning of high-performance concrete. *Cement and Concrete Research*, Vol. 32, No. 11, 2002, pp. 1699–1704.

24. de Larrard, F., and T. Sedran. Optimization of ultra-high-performance concrete by the use of a packing model. *Cement and Concrete Research*, Vol. 24, No. 6, 1994, pp. 997–1009.

25. Van, V., and H. L. Proportioning optimization of UHPC containing rice husk ash and ground granulated blast-furnace sla. 2012.

26. Nallathambi, P., B. L. Karihaloo, and B. S. Heaton. Effect of specimen and crack sizes , water / cement ratio and coarse aggregate texture upon fracture toughness of concrete. *Magazine of Concrete Research*, Vol. 36, No. 129, 1984, pp. 227–236.

27. Li, W., Q. Xu, J. Du, and J. Song. Experimental investigations for mechanical properties of reactive powder concrete under uniaxial load. *2011 International Conference on Electric Technology and Civil Engineering, ICETCE 2011 - Proceedings*, 2011, pp. 5939–5944.

28. Zollo, R. F. Fiber-reinforced concrete: An overview after 30 years of development. *Cement and Concrete Composites*, Vol. 19, No. 2, 1997, pp. 107–122.

29. Zhang, P., C. H. Liu, Q. F. Li, T. H. Zhang, and P. Wang. Fracture properties of steel fibre reinforced high-performance concrete containing nano-SiO2 and fly ash. *Current Science*, Vol. 106, No. 7, 2014, pp. 980–987.

30. Russel, G, H., and B. a. Graybeal. Ultra-High Performance Concrete : A State-of-the-Art Report for the Bridge Community. No. June, 2013, p. 171.

31. Wang, D., C. Shi, Z. Wu, J. Xiao, Z. Huang, and Z. Fang. A review on ultra high performance concrete: Part II. Hydration, microstructure and properties. *Construction and Building Materials*, Vol. 96, 2015, pp. 368–377.

32. Reda, M. M., N. G. Shrive, and J. E. Gillott. Microstructural investigation of innovative UHPC. *Cement and Concrete Research*, Vol. 29, No. 3, 1999, pp. 323–329.

33. Richard, P., and M. Cheyrezy. Composition of reactive powder concretes. *Cement and Concrete Research*, Vol. 25, No. 7, 1995, pp. 1501–1511.

34. Li, V. C. From Micromechanics to Structural Engineering. *JSCE Journal of Structural Mechanics Earthquake Eng.*, Vol. 471, No. I–24, 1993, pp. 37s-48s.

35. Ma, H., S. Qian, Z. Zhang, Z. Lin, and V. C. Li. Tailoring Engineered Cementitious Composites with local ingredients. *CONSTRUCTION & BUILDING MATERIALS*, Vol. 101, 2015, pp. 584–595.

36. Li, V. C. Postcrack Scaling relations for fiber reinforced cementitious composites. *Journal of Materials in Civil Engineering*, Vol. 4, No. 1, 1992, pp. 41–57.

37. Li, V. C. Tailoring ECC for Special Attributes: A Review. *International Journal of Concrete Structures and Materials*, Vol. 6, No. 3, 2012, pp. 135–144.

38. Li, V. C., C. Wu, S. Wang, A. Ogawa, and T. Saito. Interface Tailoring for Strain-Hardening Polyvinyl Alcohol- Engineered Cementitious Composite (PVA-ECC). *ACI Materials Journal*, Vol. 99, No. 5, 2002, pp. 463–472.

39. Marshall, D. B., & Cox, B. N. A J-integral method for calculating steady-state matrix cracking stresses in composites. *Mechanics of Materials*, Vol. 7, No. 2, 1988, pp. 127–133.

40. Yang, E. Designing Added Functions in Engineered Cementitious Composites. 2008, p. 276.

41. Kanda, T., and V. C. Li. Practical Design Criteria for Saturated Pseudo Strain Hardening Behavior in ECC. *Journal of Advanced Concrete Technology*, Vol. 4, No. 1, 2006, pp. 59–72.

42. Kanda, T., and V. C. Li. New Micromechanics Design Theory for Pseudostrain Hardening Cementitious Composites. *Journal of Engineering Mechanics*, Vol. 125, No. 4, 1999, pp. 373–381.

43. Yu, K., L. Li, J. Yu, J. Xiao, J. Ye, and Y. Wang. Feasibility of using ultra-high ductility cementitious composites for concrete structures without steel rebar. *Engineering Structures*,

Vol. 170, No. May, 2018, pp. 11–20.

44. Yu, K. Q., J. G. Dai, Z. D. Lu, and C. S. Poon. Rate-dependent tensile properties of ultra-high performance engineered cementitious composites (UHP-ECC). *Cement and Concrete Composites*, Vol. 93, No. June, 2018, pp. 218–234.

45. Yu, K. *Ultra-High Performance Engineered Cementitious Composites (UHP-ECC) - Mechanical Behavior of Material and Structural Members*. The Hong Kong Polytechnic University, 2019.

46. L, S., Z. Q, Y. K, X. F, L. P, and Z. Y. Flexural Fatigue Properties of Ultra-High Performance Engineered Cementitious Composites (UHP-ECC) Reinforced by Polymer Fibers. *Polymers*, Vol. 10, No. 8, 2018.

47. Ding, Y., J. tao Yu, K. Q. Yu, and S. lang Xu. Basic mechanical properties of ultra-high ductility cementitious composites: From 40 MPa to 120 MPa. *Composite Structures*, Vol. 185, No. July 2017, 2018, pp. 634–645.

48. Ding, Y., K. Q. Yu, J. tao Yu, and S. lang Xu. Structural behaviors of ultra-high performance engineered cementitious composites (UHP-ECC) beams subjected to bending-experimental study. *Construction and Building Materials*, Vol. 177, 2018, pp. 102–115.

49. Ranade, R., V. C. Li Prof., M. D. Stults, W. F. Heard, and T. S. Rushing. Composite properties of high-Strength, high-Ductility concrete. *ACI Materials Journal*, Vol. 110, No. 4, 2013, pp. 413–422.

50. Yu, K. Q., Z. D. Lu, J. G. Dai, and S. P. Shah. Direct Tensile Properties and Stress-Strain Model of UHP-ECC. *Journal of Materials in Civil Engineering*, Vol. 32, No. 1, 2020, pp. 1–13.

51. Zhang, Z., A. Yuvaraj, J. Di, and S. Qian. Matrix design of light weight, high strength, high ductility ECC. *Construction and Building Materials*, Vol. 210, 2019, pp. 188–197.

52. ASTM International. ASTM Standard C511 - Standard Specification for Mixing Rooms, Moist Cabinets, Moist Rooms, and Water Storage Tanks Used in the Testing of Hydraulic Cements and Concretes. *ASTM International*, 2019, pp. 1–3.

53. ASTM International. C1437 - Standard Test Method for Flow of Hydraulic Cement Mortar . *ASTM International*, 2020, pp. 1–2.

54. ASTM International. ASTM C109-20a, Standard Test Method for Compressive Strength of Hydraulic Cement Mortars (Using 2-in. or [50-mm] Cube Specimens).

55. Ranade, R. Advanced Cementitious Composite Development for Resilient and Sustainable Infrastructure. PhD thesis. 2014, p. 419.

56. He, S., J. Qiu, J. Li, and E. H. Yang. Strain hardening ultra-high performance concrete (SHUHPC) incorporating CNF-coated polyethylene fibers. *Cement and Concrete Research*, Vol. 98, 2017, pp. 50–60.

57. Japan Society of Civil Engineers. Recommendations for Design and Construction of High Performance Fiber Reinforced Cement Composites with Multiple Fine Cracks (HPFRCC).

Concrete Engineering Series, 2008, pp. 1–113.

58. Pereira, E. B., G. Fischer, J. A. O. Barros, and M. Lepech. Crack formation and tensile stress-crack opening behavior of Fiber Reinforced Cementitious Composites (FRCC). *FraMCoS-7*, 2010, pp. 1–10.

59. Zhang, Z., F. Yang, J. C. Liu, and S. Wang. Sustainable high strength, high ductility engineered cementitious composites (ECC) with substitution of cement by rice husk ash. *Cleaner Production*, Vol. 317, No. June, 2020, pp. 1–14.

60. Nematollahi, B., J. Sanjayan, and F. U. A. Shaikh. Comparative deflection hardening behavior of short fiber reinforced geopolymer composites. *Construction and Building Materials*, Vol. 70, 2014, pp. 54–64.

61. Karihaloo, B. L., and P. Nallathambi. Effective crack model for the determination of fracture toughness (KIce) of concrete. *Engineering Fracture Mechanics*, Vol. 35, No. 4–5, 1990, pp. 637–645.

62. ASTM C1609 / C1609M-19a. Standard Test Method for Flexural Performance of Fiber-Reinforced Concrete (Using Beam With Third-Point Loading). *ASTM International West Conshohocken, PA*, 2019.

63. Yu, R., P. Spiesz, and H. J. H. Brouwers. Effect of nano-silica on the hydration and microstructure development of Ultra-High Performance Concrete (UHPC) with a low binder amount. *Construction and Building Materials*, Vol. 65, 2014, pp. 140–150.

64. Juenger, M. *Effects of Supplementary Cementing Materials on the Setting Time and Early Strength of Concrete (FHWA/TX-08/0-5550-1)*. 2007.

65. Ivorra, S., P. Garcés, G. Catalá, L. G. Andión, and E. Zornoza. Effect of silica fume particle size on mechanical properties of short carbon fiber reinforced concrete. *Materials and Design*, Vol. 31, No. 3, 2010, pp. 1553–1558.

66. Gražulytė, J., A. Vaitkus, O. Šernas, and D. Čygas. Effect of silica fume on high-strength concrete performance. *World Congress on Civil, Structural, and Environmental Engineering*, No. October, 2020, pp. 1–6.

67. Sellevold, E. J., and F. F. Radjy. Condensed Silica Fume (Microsilica) in Concrete: Water Demand and Strength Development. *Special Publication*, Vol. 79, 1983, pp. 677–694.

68. Li, M., and V. C. Li. Rheology , fiber dispersion , and robust properties of Engineered Cementitious Composites. *Materials and Structures*, 2012, pp. 1–16.

69. Subedi, S., G. Arce, H. Noorvand, M. M. Hassan, M. Barbato, and L. N. Mohammad. Properties of Engineered Cementitious Composites with Raw Sugarcane Bagasse Ash used as Sand Replacement. *Journal of Materials in Civil Engineering*, Vol. In Press, 2021.